Order out of a Coulomb Phase and Higgs Transition: Frustrated Transverse Interactions of $Nd_2Zr_2O_7$

J. Xu,[1,2,*] Owen Benton,[3,†] A. T. M. N. Islam,[1] T. Guidi,[4] G. Ehlers,[5] and B. Lake[1,2,‡]
[1]Helmholtz-Zentrum Berlin für Materialien und Energie GmbH, Hahn-Meitner-Platz 1, D-14109 Berlin, Germany
[2]Institut für Festkörperphysik, Technische Universität Berlin, Hardenbergstraße 36, D-10623 Berlin, Germany
[3]RIKEN Center for Emergent Matter Science (CEMS), Wako, Saitama 351-0198, Japan
[4]ISIS facility, Rutherford Appleton Laboratory, Didcot OX11 0QX, United Kingdom
[5]Oak Ridge National Laboratory, Oak Ridge, P.O. Box 2008, Tennessee 37831, USA

(Received 25 July 2019; accepted 12 February 2020; published 6 March 2020)

The pyrochlore material $Nd_2Zr_2O_7$ with an "all-in-all-out" (AIAO) magnetic order shows novel quantum moment fragmentation with gapped flat dynamical spin ice modes. The parametrized spin Hamiltonian with a dominant frustrated ferromagnetic transverse term reveals a proximity to a U(1) spin liquid. Here we study the magnetic excitations of $Nd_2Zr_2O_7$ above the ordering temperature (T_N) using high-energy-resolution inelastic neutron scattering. We find strong spin ice correlations at zero energy with the disappearance of gapped magnon excitations of the AIAO order. It seems that the gap to the dynamical spin ice closes above T_N and the system enters a quantum spin ice state competing with and suppressing the AIAO order. Classical Monte Carlo simulations, molecular dynamics, and quantum boson calculations support the existence of a Coulombic phase above T_N. Our findings relate the magnetic ordering of $Nd_2Zr_2O_7$ with the Higgs mechanism and provide explanations for several previously reported experimental features.

DOI: 10.1103/PhysRevLett.124.097203

Competing interactions and geometrical frustration support highly degenerate states that suppress conventional magnetic order and lead to novel emergent states [1]. Classical spin ice (CSI) is a prominent example realized in $(Dy/Ho)_2Ti_2O_7$ pyrochlores consisting of a network of corner-sharing tetrahedra [2–6]. In the CSI, the single-ion Ising anisotropy due to the crystal electric field (CEF) interactions frustrates the ferromagnetic (FM) spin interactions. This creates the "2-in-2-out" (2I2O) ice rule on the spin configuration leading to infinite degeneracy [5]. In contrast, an antiferromagnetic (AFM) interaction is not frustrated resulting in a long-range "all-in-all-out" (AIAO) order [1].

Introducing transverse spin couplings, CSI transforms to quantum spin ice (QSI), allowing quantum tunneling between the degenerate ice-rule states which realizes a U(1) quantum spin liquid [7–15]. Recently, there has been a tremendous effort aimed at finding materials supporting QSI [16]. Several materials have been examined, e.g., $Yb_2Ti_2O_7$ [17], $Pr_2(Zr/Hf)_2O_7$ [18,19], and $Tb_2Ti_2O_7$ [20], but the evidence so far is ambiguous, complicated by multiphase competitions, structural defects, and low-lying crystal field levels [21–26].

As a QSI candidate, $Nd_2Zr_2O_7$ is an ideal material for modeling, having well-isolated CEF ground state Kramers doublet with Ising anisotropic, dipolar-octupolar character as well as a clean, well-ordered crystal structure [27–37]. Although it has an AIAO order below $T_N \sim 0.4$ K [29,30], it shows remarkably persistent spin dynamics [31], quantum moment fragmentation, gapped dynamical spin ice [32,35], gapped kagome spin ice in (1,1,1) fields [36], and quantum spin-1/2 chains in (1,1,0) fields [37]. The parametrized anisotropic spin-1/2 XYZ Hamiltonian based on the pseudospin-1/2 operators $\tau^{\tilde{x}}$, $\tau^{\tilde{y}}$, and $\tau^{\tilde{z}}$ describing the CEF doublet [Eq. (1)] indicates that the unfrustrated AFM $\tilde{J}_{\tilde{z}} \approx -0.046$ meV induces the AIAO order, although the FM transverse $\tilde{J}_{\tilde{x}} \approx 0.09$ meV is approximately twice as strong as $|\tilde{J}_{\tilde{z}}|$ [27,32,33,35,36]. This is a result of the frustration for the FM $\tilde{J}_{\tilde{x}}$ term.

According to linear spin wave theory, the gap to the flat spin ice modes closes at $\tilde{J}_{\tilde{x}}/|\tilde{J}_{\tilde{z}}| = 3$ [33], where spin ice configurations and AIAO order have the same energy. Classically, this signals the formation of an extensive ground-state manifold with icelike character for $\tau^{\tilde{x}}$ and the mixing of these states by quantum fluctuations caused by $\tilde{J}_{\tilde{y}}$ and $\tilde{J}_{\tilde{z}}$ stabilizes a U(1) spin liquid [33]. If there is a gapless Coulomb phase above T_N, the ordering transition would be a candidate for a Higgs transition [33]. From the viewpoint of gauge theory, QSI can be regarded as a magnetic Coulomb phase (based on $\tau^{\tilde{x}}$ for $Nd_2Zr_2O_7$) with fractionalized bosonic monopole excitations which host fluctuating U(1) gauge fields responsible for quantum electrodynamics [13]. QSI can exhibit a long-range magnetic order with respect to the transverse spin components (the AIAO order for $\tau^{\tilde{z}}$ for $Nd_2Zr_2O_7$) via a Bose-Einstein condensation of monopoles [13]. This condensation of

matter (monopole) fields coupled to gauge fields occurs through the Higgs mechanism which gaps out all soft spin excitations in the ordered state [38,39].

In this Letter, we study the magnetic excitations of $Nd_2Zr_2O_7$ above T_N using high-energy-resolution inelastic neutron scattering. We find that the gapped magnon excitations disappear and the pinch point pattern characteristic for spin ice correlations is still present but at zero energy, which points to a QSI above T_N, supporting the theoretical speculations [33]. Classical Monte Carlo (MC) simulations indicate that the system does not simply become paramagnetic with short-range AIAO correlations, but enters a intriguing state with additional strong ice correlations for $\tau^{\tilde{x}}$. Calculations for a finite temperature QSI with propagating monopole excitations are qualitatively consistent with the scattering data. Our findings shed light on the anomalously slow spin dynamics probed by muon spin relaxation commonly seen in frustrated magnets [31] and explain the puzzling temperature dependence of polarized neutron scattering data in Ref. [32].

The $Nd_2Zr_2O_7$ single crystal (~2.5 gram) was grown by using an optical floating zone furnace in the Core Laboratory for Quantum Materials in Helmholtz-Zentrum Berlin (HZB) and characterized using x-ray powder diffraction and Laue diffraction [35]. Inelastic neutron scattering experiments were conducted on the direct-geometry time-of-flight (TOF) spectrometer CNCS at SNS in Oak Ridge National Lab and on the indirect-geometry TOF spectrometer Osiris at the ISIS Neutron Source in Rutherford Appleton Lab [40,41]. For the CNCS measurement, the sample was mounted on a ^{3}He insert and neutrons of incident wavelength 4.98 Å (3.315 meV) were used in the high-flux mode (energy resolution ~0.1 meV). Data were collected at 240 mK, 450 mK, and 20 K with a 360-degree sample rotation at a step of one degree. The spin dynamics are resolved better in the Osiris experiment with an energy resolution 25 μeV [PG(200) analyzer analyzing scattered neutrons of energy 1.84 meV]. Data were collected at 30 mK, 450 mK, and 20 K using a dilution refrigerator. For both experiments, the 20 K data were used as the background. The software packages Dave [42], Mantid [43], and Horace [44] were used for data processing. Some data were averaged based on the symmetry of the scattering plane in order to improve the statistics. The MC simulations and molecular dynamics calculations were performed using the MATLAB package SpinW [45,46].

Figure 1(a) shows the constant energy slice at 0.025 meV of the CNCS data at 450 mK. It has a well-formed strong pinch point pattern but at a much lower energy than in the ordered state (~0.075 meV) [46]. Figure 1(b) presents the background-subtracted data measured on Osiris at 30 and 450 mK with a much higher energy resolution 25 μeV. Integrating over [−0.02, 0.02] meV, we see clearly a strong scattering arm along the (1,1,1) direction of the pinch point pattern at 450 mK, whereas the data at 30 mK does not show any signal except for the (2,2,0) magnetic Bragg peak. Conversely, in the data with integration over [0.06, 0.08] meV, the 450 mK data do not show a clear pattern while the data at 30 mK show the expected pinch-point spinwave modes from the AIAO order [32,35]. In Fig. 1(c), the $E-Q$ slices along the $(2,2,L)$ direction show that the gapped magnon excitations vanish above T_N and strong scattering appears around the elastic line. In addition, a weak continuum at finite energy around (2,2,0) at 450 mK is also a new feature.

In Fig. 2, we show the one-dimensional energy cuts through the Osiris data measured at 30 mK, 450 mK, and

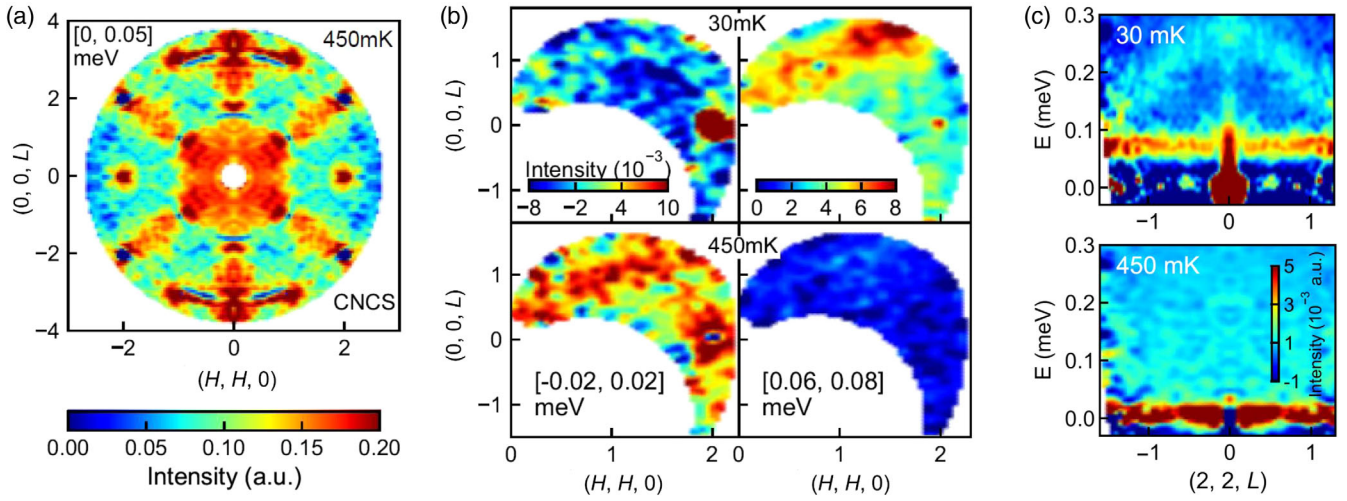

FIG. 1. (a) CNCS data at 450 mK integrated over [0, 0.05] meV (averaged according to the symmetry). (b) Comparing the 30 and 450 mK Osiris data integrated over [−0.02, 0.02] and [0.06, 0.08] meV. (c) $E-Q$ slices along the $(2,2,L)$ direction in the reciprocal space of the Osiris data at 450 and 30 mK. The data at 20 K were subtracted from both datasets. The strong sharp intensity at (2,2,0) at finite energy in the 30 mK Osiris data is an instrumental spurion resulting from leakage beyond the elastic channel.

20 K with integrating the arm of the pinch point pattern along (1,1,1) direction and at $Q = (2, 2, 0)$. Comparing with the 20 K background data, we see pronounced gapped inelastic signals at 30 mK [as well as the magnetic (2,2,0) Bragg peak] which nearly disappear at 450 mK [Figs. 2(a) and 2(c)]. After background subtraction as shown in Figs. 2(b) and 2(d), we see that most of the spectral weight becomes elastic at 450 mK. Additionally, there is an extended tail on the high energy side of the elastic peak in the cut with $Q\|(1, 1, 1)$ at 450 mK [Fig. 2(b)] which could be attributed to gapped excitations from short-range AIAO order. This is consistent with Ref. [32] where a weak broad peak with a lower energy gap was observed at 450 mK. What is more, the 450 mK data with subtracting the 30 mK data for Q along (1,1,1) illustrate clearly the shift of the pinch point pattern from ~0.07 meV below T_N to the elastic line above T_N [Fig. 2(c)].

Therefore, we can conclude that above T_N, there appears a nontrivial paramagnetic phase with significant spin-ice correlations. It is quite surprising that the strong 2I2O correlations appear just above the AIAO ordering temperature though the broad feature around the AIAO Bragg peaks at [2,2,0] and [1,1,3] in the high-temperature phase may also indicate the existence of short-range AIAO order.

To investigate the nature and origin of the high-temperature phase, we did classical MC simulations based on the anisotropic spin Hamiltonian determined in Ref. [35],

$$\mathcal{H}_{XYZ} = \sum_{\langle ij \rangle} [\tilde{J}_{\tilde{x}} \tau_i^{\tilde{x}} \tau_j^{\tilde{x}} + \tilde{J}_{\tilde{y}} \tau_i^{\tilde{y}} \tau_j^{\tilde{y}} + \tilde{J}_{\tilde{z}} \tau_i^{\tilde{z}} \tau_j^{\tilde{z}}], \qquad (1)$$

where $\tau_i^{\tilde{\alpha}}$ $(\alpha = x,\ y,\ z)$ is the α component of the pseudospin-1/2 at site i defined in the rotated local frames and $\tilde{J}_{\tilde{\alpha}}$ is the corresponding nearest-neighbor exchange constant [27,33]. The calculations were done using the exchange interaction parameters given in Ref. [35] with a supercell of $6 \times 6 \times 6$ cubic unit cells (3456 spins) [46]. The simulated specific heat indicates that the system enters the AIAO phase at a theoretical Neél temperature $T'_N \approx 0.18$ K (lower than the experimental one possibly due to quantum effects stabilizing the order). Above T'_N at 0.25 K the calculated neutron scattering structure factor [Fig. 3(a)] shows a pinch point pattern coexisting with broad signals around the AIAO Bragg peak wave vectors [2,2,0] and [1,1,3], which is quite consistent with the experiment [Fig. 1(a)].

To identify the spin correlations responsible for this novel scattering pattern, we calculated the thermal average of the amplitudes of the pseudospin components, $\langle|\tau^{\tilde{\alpha}}|\rangle$ $(\alpha = x,\ y,\ z)$ and the probability distribution functions (pdfs) of $\tau^{\tilde{\alpha}}$ and the average over tetrahedra $1/4 \sum_{\boxtimes} \tau^{\tilde{\alpha}}$. Figure 3(b) shows the temperature dependence of $\langle|\tau^{\tilde{\alpha}}|\rangle$. At base temperature, only $\langle|\tau^{\tilde{z}}|\rangle$ is significant consistent with the AIAO order. With increasing temperature, $\langle|\tau^{\tilde{z}}|\rangle$ decreases while $\langle|\tau^{\tilde{x}}|\rangle$ and $\langle|\tau^{\tilde{y}}|\rangle$ increase due to enhanced thermal fluctuations and all approach $\tau/2 = 0.25$ ($\tau = 1/2$ is the amplitude of pseudospin) as expected for a completely random spin configuration. Remarkably, above T'_N, $\langle|\tau^{\tilde{x}}|\rangle$ is greater than both the thermal average $\tau/2$ and

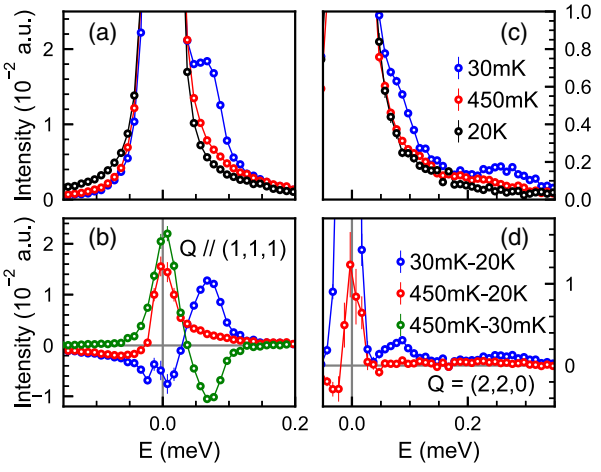

FIG. 2. Cuts through the Osiris data at 30 mK, 450 mK, and 20 K (upper panels) and subtracted data 30 mK–20 K, 450 mk–20 K, and 450–30 mK [only for (b)] (lower panels). The data are integrated along $Q\|(1, 1, 1)$ [excluding the (1,1,1) Bragg peak] with a width 0.2(r.l.u.) over $(1, 1, -2)$ [(a) and (b)] and around $Q = (2, 2, 0)$ [(c) and (d)]. The gray lines in (b) and (c) denote the zeros of the axes.

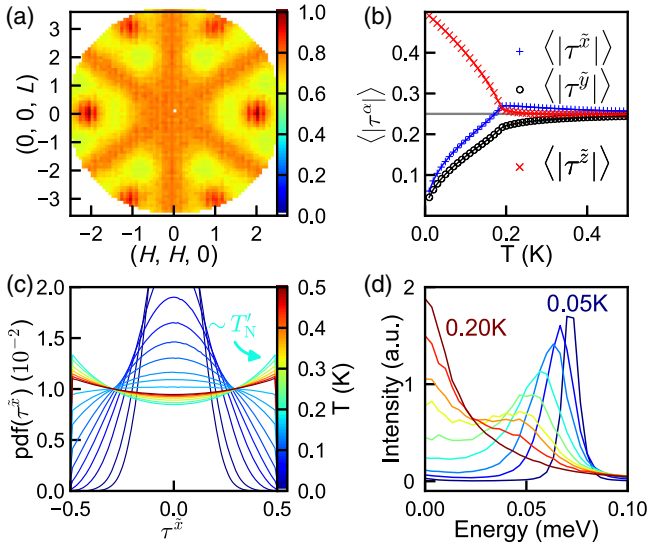

FIG. 3. Results of Monte Carlo simulations. (a) Neutron scattering structure factor (equal-time correlations) at 0.25 K. (b) Temperature dependence of $\langle|\tau^{\tilde{\alpha}}|\rangle$ (the gray horizontal line shows the expected $\tau/2$ for a random spin configuration). (c) Probability distribution functions of $\tau^{\tilde{x}}$ $(-0.5 \le \tau^{\tilde{\alpha}} \le 0.5$ for the spin-1/2 system). See the Supplemental Material [46] for corresponding figures for $\tau^{\tilde{y}}$ and $\tau^{\tilde{z}}$. (d) Evolution of the gapped flat mode for several temperatures (0.05, 0.1, 0.125, 0.15, 0.165, 0.175, 0.18, 0.185, 0.2 K) simulated using semiclassical molecular dynamics averaging over Q from (0.1,0.1,0) to (0.9,0.9,0) [46].

$\langle|\tau^{\tilde{z}}|\rangle$, and then decays slowly with increasing temperature exhibiting a maximum around T'_N. By contrast, $\langle|\tau^{\tilde{z}}|\rangle$ decreases quickly and even becomes slightly lower than $\tau/2$, revealing the breakdown of the AIAO correlations.

We characterize the correlations of $\tau^{\tilde{x}}$ with the probability distribution functions mentioned above. As shown in Fig. 3(c), at temperatures below T'_N, pdf$(\tau^{\tilde{x}})$ is a Gaussian function centered at zero and its width increases with raising temperature. Above T'_N, it surprisingly develops two maxima at $\pm\tau$ decaying with further increasing temperature, which means that $\tau^{\tilde{x}}$ points into the tetrahedron for half of the spins and out of the tetrahedron for the other half. Pdf$(1/4\sum_{\boxtimes}\tau^{\tilde{x}})$ shows how the in/out $\tau^{\tilde{x}}$ is distributed on the tetrahedra which is always a Gaussian function at zero (shown in Ref. [46]). The above two statistical quantities indicate that ice-rule correlations appear for $\tau^{\tilde{x}}$ on the tetrahedra consistent with the FM $\tilde{J}_{\tilde{x}}$. On the other hand, pdf$(\tau^{\tilde{z}})$ and pdf$(1/4\sum_{\boxtimes}\tau^{\tilde{z}})$ change from peaks at either τ or $-\tau$ (depending on the AIAO domain type) to be a broad peak at zero with increasing temperature indicating the loss of the AIAO correlations of $\tau^{\tilde{z}}$ [46].

Both experiments and classical MC simulations reveal strong spin ice correlations above T_N. Assuming the existence of a Coulomb phase with respect to $\tau^{\tilde{x}}$ above T_N, we have calculated the correlations based on the bosonic many-body theory of QSI [46,47]. As shown in Fig. 4, the calculated dynamical structure factor at 450 mK (integrated over [0, 0.05] meV) exhibits a pinch point pattern with additional broad scattering around [2,2,0] and [1,1,3] in good agreement with experimental data. Besides the pinch point pattern at zero energy due to the scattering of the Coulomb phase, monopole creation and hopping cause broad scattering around [2,2,0] and [1,1,3]. Neutrons can be scattered by monopoles via two different processes: (i) the incoming neutron flips a spin belonging to an ice-rule tetrahedron creating a pair of monopoles, which gives a continuum at finite energy above a small gap; (ii) at finite temperature where there is a finite density of monopoles already in the system, the incoming neutron can flip a spin belonging to a monopole tetrahedron causing this monopole to hop which gives a continuum of scattering around zero energy. These scattering features are shown in Fig. 4(b). This agrees with our data which exhibit strong broad signals around [2,2,0] and [1,1,3] at zero energy and a continuum at finite energy. However, the gapped feature expected around [2,2,0] and [1,1,3] is not clear in the data which could be attributed to possible fast decay of the coherent monopole excitations due to, for example, strong thermal fluctuations. The signal also may be contaminated by the scattering from possible short-range AIAO correlations.

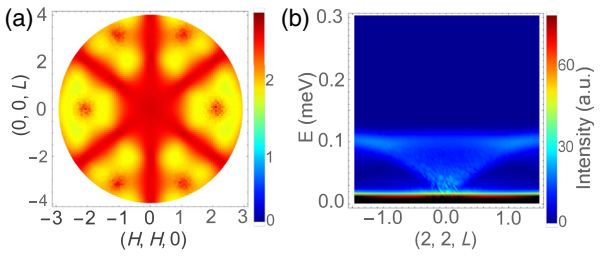

FIG. 4. (a) Calculated neutron scattering pattern at 450 mK of the magnetic Coulomb phase based on $\tau^{\tilde{x}}$ according to the classical theory in Ref. [6] and monopoles using the quantum theory in Ref. [47] where the pinch point pattern is caused by the divergence-free Coulomb phase and the broad signals at $Q = [2, 2, 0]$ and [1,1,3] are due to monopoles. (b) $E - Q$ plot along $(2, 2, L)$ showing the scattering continuum due to monopole hopping (elastic) and creation (inelastic) at 450 mK. Energy resolutions 0.1 and 0.02 meV were included for (a) and (b), respectively.

The existence of strong gapless spin-ice correlations for $\tau^{\tilde{x}}$ above T_N which become gapped flat dynamical spin-ice modes in the $\tau^{\tilde{z}}$-ordered state below T_N [32,35] makes the ordering a candidate for a Higgs transition where the emergent gauge field of the Coulomb phase above T_N is gapped by the condensation of emergent gauge charges (monopoles) [39,48]. Our semiclassical molecular dynamics calculations [Fig. 3(d) and Ref. [46]] show that the gap closes with raising temperature which supports this picture. A Higgs transition was also proposed for pyrochlore $Yb_2Ti_2O_7$ by demonstrating the first order nature of the ordering transition and the sudden suppression of the intensity of the pinch point pattern below the transition [48]. The gapped and gapless pinch point patterns below and above T_N is further important evidence for a Higgs transition.

Our results provide an explanation for the seemingly contradictory temperature dependences of the intensities of the AIAO Bragg peak and the pinch point pattern in the energy-integrated polarized neutron scattering data reported for $Nd_2Zr_2O_7$ [32] and very recently for Nd_2ScNbO_7 [49]. It was shown that with increasing temperature, the magnetic Bragg peak weakens and disappears at T_N while the pinch point intensity maximizes around T_N and persists to much higher temperatures ($\sim$1 K) for both compounds. This cannot be rationalized if the pinch point scattering is only a feature of the magnons in the ordered state. We argue that at T_N the gapped pinch point pattern is replaced by a pinch point pattern at zero energy due to the Coulomb phase built on $\tau^{\tilde{x}}$ which has the strongest ice correlations around T_N and gets weaker slowly with increasing temperature, similar to the temperature evolution of $\langle|\tau^{\tilde{x}}|\rangle$ in the MC simulations [Fig. 3(b)]. The temperature range where the pinch point pattern presents is also comparable with the strength of $\tilde{J}_{\tilde{x}}$. In addition, the Coulomb phase with strongly correlated spins could induce slow spin dynamics which supports the observed anomalously slow paramagnetic spin dynamics in the muon spin relaxation experiments [31].

Furthermore, it was reported that a spin ice model with frustrated transverse terms exhibits competing phases and nematicity [50,51]. Our results provide an experimental and theoretical example of an Ising antiferromagnet with frustrated transverse terms which also shows interesting physics. Our further MC simulations [46] show that the ordering temperature is strongly suppressed with increasing $\tilde{J}_{\tilde{x}}/|\tilde{J}_{\tilde{z}}|$, which should be constant in the mean field theory and the ordered phase invades the spin ice phase at finite temperature for $\tilde{J}_{\tilde{x}}/|\tilde{J}_{\tilde{z}}| > 3$ similar to the phase diagram in Ref. [50], which is surprising because the spin ice phase should be more stable due to the higher entropy. Further theoretical study is needed.

In summary, we used inelastic neutron scattering, classical MC simulations, semiclassical molecular dynamics simulations, and a bosonic theory to show that $Nd_2Zr_2O_7$ has a nontrivial paramagnetic state with spin-ice correlations, which is possibly a magnetic Coulomb phase, despite an AIAO ordered ground state. We attributed to the dominant frustrated transverse $\tilde{J}_{\tilde{x}}$ term in the spin Hamiltonian and related the ordering transition to the Higgs mechanism. Our results indicate that the paramagnetic phase of an ordered system may host unconventional spin correlations different from the ground-state order in nature due to competition and frustration among different terms of anisotropic exchange interactions. This expands the field for searching for QSI to ordered systems with frustrated terms in the spin Hamiltonian and makes it interesting to examine several similar QSI candidates with AIAO order, such as $Nd_2(Hf/Sn/Pb)_2O_7$, Nd_2ScNbO_7, and $Sm_2(Ti/Sn)_2O_7$ [49,52–56].

We thank K. Siemensmeyer, Y.-P. Huang, M. Hermele, S. T. Bramwell, and A. T. Boothroyd for helpful discussions on the related theory. This research was supported by the DFG through Project B06 of SFB 1143 (Project-id 247310070). This research used resources at the Spallation Neutron Source, a DOE Office of Science User Facility operated by the Oak Ridge National Laboratory. Experiments at the ISIS Neutron and Muon Source were supported by a beam time allocation RB1810504 from the Science and Technology Facilities Council (DOI: 10.5286/ISIS.E.92924095).

*jianhui.xu@helmholtz-berlin.de
†john.benton@riken.jp
‡bella.lake@helmholtz-berlin.de

[1] C. Lacroix, P. Mendels, and F. Mila, *Introduction to Frustrated Magnetism: Materials, Experiments, Theory* (Springer Science and Business Media, New York, 2011), Vol. 164.
[2] J. S. Gardner, M. J. P. Gingras, and J. E. Greedan, Rev. Mod. Phys. **82**, 53 (2010).
[3] T. Fennell, P. P. Deen, A. R. Wildes, K. Schmalzl, D. Prabhakaran, A. T. Boothroyd, R. J. Aldus, D. F. McMorrow, and S. T. Bramwell, Science **326**, 415 (2009).
[4] D. J. P. Morris, D. A. Tennant, S. A. Grigera, B. Klemke, C. Castelnovo, R. Moessner, C. Czternasty, M. Meissner, K. C. Rule, J.-U. Hoffmann, K. Kiefer, S. Gerischer, D. Slobinsky, and R. S. Perry, Science **326**, 411 (2009).
[5] M. J. Harris, S. T. Bramwell, D. F. McMorrow, T. Zeiske, and K. W. Godfrey, Phys. Rev. Lett. **79**, 2554 (1997).
[6] C. L. Henley, Phys. Rev. B **71**, 014424 (2005).
[7] M. Hermele, M. P. A. Fisher, and L. Balents, Phys. Rev. B **69**, 064404 (2004).
[8] N. Shannon, O. Sikora, F. Pollmann, K. Penc, and P. Fulde, Phys. Rev. Lett. **108**, 067204 (2012).
[9] L. Savary and L. Balents, Phys. Rev. Lett. **108**, 037202 (2012).
[10] S. Onoda and Y. Tanaka, Phys. Rev. Lett. **105**, 047201 (2010).
[11] S. Onoda and Y. Tanaka, Phys. Rev. B **83**, 094411 (2011).
[12] O. Benton, O. Sikora, and N. Shannon, Phys. Rev. B **86**, 075154 (2012).
[13] S. B. Lee, S. Onoda, and L. Balents, Phys. Rev. B **86**, 104412 (2012).
[14] Y. Kato and S. Onoda, Phys. Rev. Lett. **115**, 077202 (2015).
[15] C. J. Huang, Y. Deng, Y. Wan, and Z. Y. Meng, Phys. Rev. Lett. **120**, 167202 (2018).
[16] M. J. P. Gingras and P. A. McClarty, Rep. Prog. Phys. **77**, 056501 (2014).
[17] K. A. Ross, L. Savary, B. D. Gaulin, and L. Balents, Phys. Rev. X **1**, 021002 (2011).
[18] K. Kimura, S. Nakatsuji, J.-J. Wen, C. Broholm, M. B. Stone, E. Nishibori, and H. Sawa, Nat. Commun. **4**, 1934 (2013).
[19] R. Sibille, N. Gauthier, H. Yan, M. C. Hatnean, J. Ollivier, B. Winn, U. Filges, G. Balakrishnan, M. Kenzelmann, N. Shannon, and T. Fennell, Nat. Phys. **14**, 711 (2018).
[20] J. S. Gardner, S. R. Dunsiger, B. D. Gaulin, M. J. P. Gingras, J. E. Greedan, R. F. Kiefl, M. D. Lumsden, W. A. MacFarlane, N. P. Raju, J. E. Sonier, I. Swainson, and Z. Tun, Phys. Rev. Lett. **82**, 1012 (1999).
[21] L. D. C. Jaubert, O. Benton, J. G. Rau, J. Oitmaa, R. R. P. Singh, N. Shannon, and M. J. P. Gingras, Phys. Rev. Lett. **115**, 267208 (2015).
[22] H. Yan, O. Benton, L. Jaubert, and N. Shannon, Phys. Rev. B **95**, 094422 (2017).
[23] N. Martin, P. Bonville, E. Lhotel, S. Guitteny, A. Wildes, C. Decorse, M. Ciomaga Hatnean, G. Balakrishnan, I. Mirebeau, and S. Petit, Phys. Rev. X **7**, 041028 (2017).
[24] J. J. Wen, S. M. Koohpayeh, K. A. Ross, B. A. Trump, T. M. McQueen, K. Kimura, S. Nakatsuji, Y. Qiu, D. M. Pajerowski, J. R. D. Copley, and C. L. Broholm, Phys. Rev. Lett. **118**, 107206 (2017).
[25] H. R. Molavian, M. J. P. Gingras, and B. Canals, Phys. Rev. Lett. **98**, 157204 (2007).
[26] A. J. Princep, H. C. Walker, D. T. Adroja, D. Prabhakaran, and A. T. Boothroyd, Phys. Rev. B **91**, 224430 (2015).
[27] Y.-P. Huang, G. Chen, and M. Hermele, Phys. Rev. Lett. **112**, 167203 (2014).

[28] M. C. Hatnean, M. R. Lees, O. A. Petrenko, D. S. Keeble, G. Balakrishnan, M. J. Gutmann, V. V. Klekovkina, and B. Z. Malkin, Phys. Rev. B **91**, 174416 (2015).
[29] E. Lhotel, S. Petit, S. Guitteny, O. Florea, M. C. Hatnean, C. Colin, E. Ressouche, M. R. Lees, and G. Balakrishnan, Phys. Rev. Lett. **115**, 197202 (2015).
[30] J. Xu, V. K. Anand, A. K. Bera, M. Frontzek, D. L. Abernathy, N. Casati, K. Siemensmeyer, and B. Lake, Phys. Rev. B **92**, 224430 (2015).
[31] J. Xu, C. Balz, C. Baines, H. Luetkens, and B. Lake, Phys. Rev. B **94**, 064425 (2016).
[32] S. Petit, E. Lhotel, B. Canals, M. C. Hatnean, J. Ollivier, H. Mutka, E. Ressouche, A. R. Wildes, M. R. Lees, and G. Balakrishnan, Nat. Phys. **12**, 746 (2016).
[33] O. Benton, Phys. Rev. B **94**, 104430 (2016).
[34] L. Opherden, J. Hornung, T. Herrmannsdörfer, J. Xu, A. T. M. N. Islam, B. Lake, and J. Wosnitza, Phys. Rev. B **95**, 184418 (2017).
[35] J. Xu, O. Benton, V. K. Anand, A. T. M. N. Islam, T. Guidi, G. Ehlers, E. Feng, Y. Su, A. Sakai, P. Gegenwart, and B. Lake, Phys. Rev. B **99**, 144420 (2019).
[36] E. Lhotel, S. Petit, M. C. Hatnean, J. Ollivier, H. Mutka, E. Ressouche, M. R. Lees, and G. Balakrishnan, Nat. Commun. **9**, 3786 (2018).
[37] J. Xu, A. T. M. N. Islam, I. N. Glavatskyy, M. Reehuis, J.-U. Hoffmann, and B. Lake, Phys. Rev. B **98**, 060408(R) (2018).
[38] E. Fradkin and S. H. Shenker, Phys. Rev. D **19**, 3682 (1979).
[39] S. Powell, Phys. Rev. B **84**, 094437 (2011).
[40] G. Ehlers, A. A. Podlesnyak, and A. I. Kolesnikov, Rev. Sci. Instrum. **87**, 093902 (2016).
[41] M. T. F. Telling and K. H. Andersen, Phys. Chem. Chem. Phys. **7**, 1255 (2005).
[42] C. M. Brown, J. R. D. Copley, and R. M. Dimeo, J. Res. Natl. Inst. Stand. Technol. **114**, 341 (2009).
[43] O. Arnold *et al.*, Nucl. Instrum. Methods Phys. Res., Sect. A **764**, 156166 (2014).
[44] R. A. Ewings, A. Buts, M. D. Le, J. van Duijn, I. Bustinduy, and T. G. Perring, Nucl. Instrum. Methods Phys. Res., Sect. A **834**, 132 (2016).
[45] S. Toth and B. Lake, J. Phys. Condens. Matter **27**, 166002 (2015).
[46] See Supplemental Material at http://link.aps.org/supplemental/10.1103/PhysRevLett.124.097203 for more data analyses and calculation details.
[47] Z. Hao, A. G. R. Day, and M. J. P. Gingras, Phys. Rev. B **90**, 214430 (2014).
[48] L.-J. Chang, S. Onoda, Y. Su, Y.-J. Kao, K.-D. Tsuei, Y. Yasui, K. Kakurai, and M. R. Lees, Nat. Commun. **3**, 992 (2012).
[49] C. Mauws, N. Hiebert, M. Rutherford, H. D. Zhou, Q. Huang, M. B. Stone, N. P. Butch, Y. Su, E. S. Choi, Z. Yamani, and C. R. Wiebe, arXiv:1906.10763.
[50] M. Taillefumier, O. Benton, H. Yan, L. D. C. Jaubert, and N. Shannon, Phys. Rev. X **7**, 041057 (2017).
[51] O. Benton, L. D. C. Jaubert, R. R. P. Singh, J. Oitmaa, and N. Shannon, Phys. Rev. Lett. **121**, 067201 (2018).
[52] V. K. Anand, A. K. Bera, J. Xu, T. Herrmannsdörfer, C. Ritter, and B. Lake, Phys. Rev. B **92**, 184418 (2015).
[53] A. Bertin, P. D. de Réotier, B. Fåk, C. Marin, A. Yaouanc, A. Forget, D. Sheptyakov, B. Frick, C. Ritter, A. Amato, C. Baines, and P. J. C. King, Phys. Rev. B **92**, 144423 (2015).
[54] A. M. Hallas, A. M. Arevalo-Lopez, A. Z. Sharma, T. Munsie, J. P. Attfield, C. R. Wiebe, and G. M. Luke, Phys. Rev. B **91**, 104417 (2015).
[55] C. Mauws, A. M. Hallas, G. Sala, A. A. Aczel, P. M. Sarte, J. Gaudet, D. Ziat, J. A. Quilliam, J. A. Lussier, M. Bieringer, H. D. Zhou, A. Wildes, M. B. Stone, D. Abernathy, G. M. Luke, B. D. Gaulin, and C. R. Wiebe, Phys. Rev. B **98**, 100401(R) (2018).
[56] V. Peçanha-Antonio, E. Feng, X. Sun, D. Adroja, H. C. Walker, A. S. Gibbs, F. Orlandi, Y. Su, and T. Brckel, Phys. Rev. B **99**, 134415 (2019).